Film Formation of Poly (methyl methacrylate) Latex With Pyrene Functional Poly (divinylbenzene) Microspheres Prepared by Click Chemistry

Şaziye Uğur,[1] Önder Yargı,[1] Yasemin Yüksel Durmaz,[2] Bünyamin Karagöz,[2] Niyazi Bıçak,[2] Yusuf Yağcı,[2] Önder Pekcan[3]

[1]Department of Physics, Istanbul Technical University, Maslak, 34469, Istanbul, Turkey

[2]Department of Chemistry, Istanbul Technical University, Maslak, 34469, Istanbul, Turkey

[3]Faculty of Arts and Science, Kadir Has University, Cibali, 34320, Istanbul, Turkey

This work reports on the application of steady state fluorescence (SSF) technique for studying film formation from poly(methyl methacrylate) (PMMA) latex and poly(divinylbenzene) (PDVB) microsphere composites. Pyrene (P) functionalized PDVB cross-linked spherical microspheres with diameters of 2.5 μm were synthesized by using precipitation polymerization technique followed by click coupling reaction. The diameter of the PMMA particles prepared by emulsion polymerization were in the range of 0.5–0.7 μm. PMMA/PDVB composite films were then prepared by physically blending of PMMA latex with PDVB microspheres at various composition (0, 1, 3, 5, 10, 20, 40, and 60 wt%). After drying, films were annealed at elevated temperatures above T_g of PMMA ranging from 100 to 270°C for 10 min time intervals. Evolution of transparency of the composite films was monitored by using photon transmission intensity, I_{tr}. Monomer (I_P) and excimer (I_E) fluorescence intensities from P were measured after each annealing step. The possibility of using the excimer-to-monomer intensity ratio (I_E/I_P) from PDVB microparticles as a measure of PMMA latex coalescence was demonstrated. Diffusion of the PMMA chains across the particle–particle interfaces dilutes the dyes, increasing their separation. The film formation stages of PMMA latexes were modeled by monitoring the I_E/I_P ratios and related activation energies were determined. There was no observable change in activation energies confirming that film formation behavior is not affected by varying the PDVB composition in the studied range. SEM images of PMMA/PDVB composites confirmed that the PMMA particles undergo complete coalescence forming a continuous phase in where PDVB microspheres are dispersed. POLYM. COMPOS., 32:869–881, 2011. © 2011 Society of Plastics Engineers

INTRODUCTION

A number of methods including water-based emulsion, seeded suspension, nonaqueous dispersion polymerization, and precipitation polymerization were successfully employed for the preparation of monodisperse microspheres [1–4]. Among them, precipitation polymerization, which can be performed in the absence of any added surfactant or stabilizer [5–12] appeared to be an attractive route to obtain microspheres with uniform size and shape. Typically, monodisperse and highly crosslinked poly(divinylbenzene) (PDVB) surfactant-free microspheres (with diameters between 2 and 5 μm) were prepared by using only monomer (commercial divinylbenzene, DVB55), radical initiator (2, 2′-azobisisobutronitrile, AIBN), and solvent (acetonitrile) [5]. Interestingly, PDVB microspheres formed in this method contained significant residual double bonds in the particle and on the surface of the particle [13]. The residual double bonds located at the surface permitted further growth and modification of particles.

The "click reactions" [14, 15], in particular Cu(I)-catalyzed 1,3-dipolar Huisgen cycloaddition reactions between an azide and an alkyne, have gained a great deal of attention due to their high specificity and nearly quantitative yields in the presence of many functional groups. Recently, PDVB microspheres were functionalized [16] by polymeric chains using two click reactions, namely thiol-ene chemistry and azide-alkyne cycloaddition reaction. We also reported functionalization of PDVB microspheres by the copper-catalyzed Huisgen 1-3 dipolar cycloaddition click reaction with a small fluorescent molecule-alkyne modified pyrene [17].

Polymer composites are often prepared by mixtures of two or more different kinds of particles in the dispersed state. Upon drying of the dispersion, both types of particles

contribute to the properties of the film that is formed. Composite materials form a class of materials in which immiscible compounds are combined in order to obtain new properties [18]. They are heterogeneous mixtures of their components which are generally of quite different properties. Their properties often depart very much from those of the pure components, so that mixing two homogeneous materials into a composite really results in the formation of a new material. Properties depend much more on the morphology and adhesion properties at the interfaces than on the volume fraction of each phase as would happen in an ideal mixture. Several authors have examined the properties of hard/soft latex blends. Hard refers to particles consisting of a polymer with a T_g above room temperature, and soft refers to particles of a low-T_g polymer. As a result of worldwide theoretical and experimental efforts, a very good understanding of the mechanisms of latex film formation has been achieved [19–23]. Traditionally, the film formation process of pure polymer latex is considered in terms of three sequential steps: (i) water evaporation and subsequent packing of polymer particles (ii) deformation of the particles and close contact between the particles if their T_g is less than or close to the drying temperature (soft or low T_g latex). Latex with a T_g above the drying temperature (hard or high T_g latex) stays undeformed at this stage. In the annealing of hard latex system, deformation of particles first leads to void closure [24, 25] and then after the voids disappear, diffusion across particle-particle boundaries starts, i.e. the mechanical properties of hard latex films evolve during annealing, after all solvent has evaporated and all voids have disappeared. (iii) Coalescence of the deformed particles to form a homogeneous film [25] where macromolecules belonging to different particles mix by interdiffusion [26, 27]. However, the film formation process of composite latex is more complicated than homogeneous one due to the interactions between the different phases. In addition, several factors such as molecular weight and its distribution, synthetic methodology, morphologies of latex particles, stabilizers, surfactants, annealing, film formation conditions, etc. were experimentally shown to influence composite latex film formation [28–32].

Commercial plastics and rubbers are often filled with solid particles, either to enhance their mechanical properties or to reduce cost [33]. The properties of these materials depend primarily on the interactions between the matrix and the filler particles, although interparticle interactions are also important [34]. Consequently, the influence of physical interactions on the rheology of filled polymers can be very complex [35, 36]. Strong interactions between the matrix polymer and the filler particles can increase the viscosity and the dynamic moduli, for example through adsorption of the polymer on the filler surface restricting chain mobility within the matrix. The nature and surface composition of the particles, as well as matrix properties such as the polarity and the molecular weight influence the rheology of the mixtures. While much effort has been devoted to investigating the influence of filler surface treatment on the rheological behavior of filled polymers, most studies have used commercial fillers such as carbon black, calcium carbonate, mica, and talc [37–39]. These fillers often have a complex structure and generally form aggregated suspensions with poorly characterized particle-matrix interactions impeding the interpretation of the rheological results. The influence on melt rheology of model cross-linked fillers has been investigated by simple dispersion of the particles in different matrices [40–43], by incorporation of the particles into the matrix network through covalent bonding [44], and by adding a shell to enhance filler compatibility with the matrix [45–48]. The importance of gelled rubber, as a component in rubber formulations for improved processing has increased in the last decades. Improvements in processing, however, are usually obtained at the expense of certain physical properties of the finished product. This drawback has been overcome by latex blending, where crosslinked particles of colloidal size were reported to successfully reinforce various rubbers and plastics [49]. Such a mixing route results in a good degree of dispersion of the gel. It has been pointed out that reinforcement practically occurs only with latex blending.

Fluorescence technique provides useful information about the environment of fluorophores on much smaller length scale (a few nanometers) and, therefore, can be used to establish whether two polymers are mixed on a molecular level. In some applications of fluorescence, it is often advantageous to design the experiment so that one can monitor two separate emissions at different wavelengths. This approach provides increased accuracy because one signal can act as a reference, or the two signals may be coupled in a well-understood way so that information can be obtained from the ratio of intensities. In a series of articles from Winter's group [50, 51] the results of studies of blends containing polystyrene plus poly(vinyl methyl ether) in a shear flow with a modified rheometer with fluorescence measurement capabilities are described. Morawetz et al. [52, 53] pioneered the application of nonradiative energy transfer (ET) method to the study of miscibility in polymer blends. In this technique, one of the polymers is labeled with a fluorescence donor, and the other is labeled with a fluorescence acceptor. When the two polymers are miscible, the donors and acceptors are spatially close, and ET from donor to acceptor can take place. This process results in a decrease of donor fluorescence intensity, accompanied by an increase in the fluorescence intensity of the acceptor.

The fluorescence spectrum of pyrene consist of two components; there is a structured emission band between 370 and 450 nm which is characteristic of excited monomer molecules and a structureless red shifted, broad band. This blue emission band originates from excited dimers called excimer, formed by the association of excited and unexcited monomer molecules [54]. As the concentration of pyrene molecules is increased, the monomer intensity, I_P, of pyrene monomer decreases and the excimer inten-
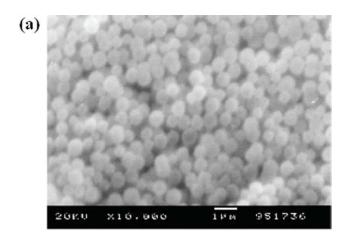
sity, I_E, increases. The I_E/I_P is proportional to the pyrene concentration [55]. The absorption spectrum is independent of pyrene concentration and is characteristic of the monomer, showing that the dimers are not present in the ground state. Pyrene excimer formation was used to probe the end-to-end cyclization dynamics in polymers [56, 57]. The morphology of non-aqueous particles was studied by using pyrene excimer formation method by labeling particles with pyrene molecules [58]. In our previous studies, we have studied film formation behaviors of latex blends with different T_g values which undergo mixing as a consequence of polymer diffusion across the boundary between neighboring cells in a blend film [59–62]. The rate and extent of polymer diffusion was monitored through fluorescence measurements, where the one of latexes are labeled with pyrene.

The objective of this work was to study the film forming ability of PMMA latex and PDVB microsphere composite depending on their weight fraction by means of fluorescence and UVV techniques. Films were prepared by physically blending of PMMA and PDVB particles, the latter being crosslinked and labeled with pyrene (P). Different compositions of composites were prepared and annealed above the glass transition temperature of PMMA ranging from 100 to 270°C for 10 min. The evolution of film formation from PMMA/PDVB composite was studied by monitoring monomer (I_P) and excimer (I_E) emission intensities from PDVB. Transmitted photon intensity, I_{tr} was also monitored to study the evolution of transparency in composite films. The surface morphologies are examined with scanning electron microscopy (SEM). The changes in I_{tr} and I_E/I_P ratio by increasing the annealing temperatures were attributed to the void-closure and interdiffusion processes. Film formation stages were modeled and related activation energies were obtained.

EXPERIMENT

Particle Preparation

Synthesis of PMMA Latex. Unlabeled PMMA latex particles were prepared in a two-step process [63–65]. First MMA was polymerized to low conversion in cyclohexane in the presence of polyisobutylene (PIB) containing 2% isoprene units to promote grafting. The graft copolymer so produced served as a dispersant in the second stage of polymerization, in which MMA was polymerized in a cyclohexane solution of the polymer. This material, the dispersant, was collected and purified by precipitation with methanol. The dispersant was then added to a second reaction vessel containing cyclohexane, AIBN, and MMA. These solutions were refluxed overnight. The reaction became increasingly turbid as it progressed. The latex particles were separated from the solvent and unreacted monomers by repeated cycles of centrifugation, the supernatant liquid was decanted, and the latex particles were
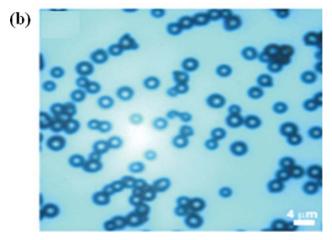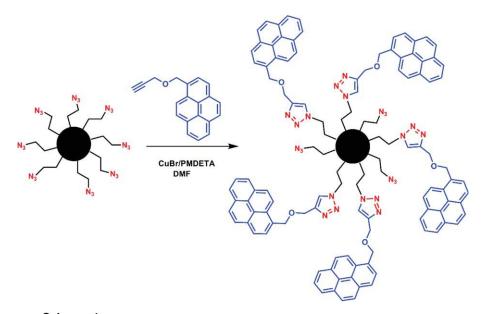

FIG. 1. (a) SEM image of the PMMA particles, (b) Optical microscope image of azide functionalized PDVB microspheres. [Color figure can be viewed in the online issue, which is available at wileyonlinelibrary.com.]

redispersed in fresh solvent. These latex dispersions in cyclohexane could be separately freeze-dried and stored as a powder. The produced stable dispersions of spherical polymer latexes range in radius from 0.5 to 0.7 μm (see Fig. 1a). A combination of ^{1}H NMR and UV analysis indicates that these particles contain 4 mol% PIB (These particles were prepared in Professor M. A.Winnik's Laboratory in Toronto). The molecular weight of graft PMMA was measured as $M_w = 1.10 \times 10^5$ and the polydispersity of the PMMA was 2.3.

Synthesis of Pyrene Functionalized PDVB Microspheres. PDVB microspheres were synthesized via click chemistry strategy [17]. Divinylbenzene (DVB55, 55% mixture of isomers, technical grade, Aldrich) was used as received. Acetonitrile (99%, Aldrich) was distilled over CaH_2 before use. 2, 2′-Azobis (isobutyronitrile)(AIBN, Fluka) was recrystallized from methanol. N,N, N′, N″, N″-pentamethyldiethylenetriamine (PMDETA, 99%, Aldrich) as a ligand was distilled before use. Dichloromethane (CH_2Cl_2, 99% Lab-Scan) was distilled over P_2O_5. N,N-Dimethylformamide (DMF, ≥99%, Aldrich), sulfuric acid (95–97%, Fluka), potassium bromide (≥99.5%, Merck), so-

Scheme 1. Synthesis of pyrene functionalized PDVB microspheres via click chemistry.

dium azide (≥99%, Merck), sodium chromate (Merck), silver nitrate (Merck), CuBr (98%, Acros), sodium hydride (98%, Fluka), propargyl bromide (80 vol% in toluene, Fluka), 1-pyrene methanol (98%, Aldrich), methanol (99%, Reiden-de Haön), diethylether (98%, Carlo-Erba) and tetrahydrofuran (THF, 99% Lab-Scan) were used as received.

PDVB microspheres were prepared by precipitation polymerization technique as described in the literature [5]. For this purpose, AIBN (0.2 g, 1.22 mmol, 4 wt% relative to DVB55) was added to the solution of DVB55 (11 mL, 76.8 mmol, 4 vol% relative to total volume) and 274 mL acetonitrile in dry 500 mL volume of three-necked flask equipped with a mechanical stirrer and a nitrogen inlet. The flask was placed in thermostated oil bath and the temperature was adjusted to 70°C. The nitrogen flow was stopped and the reaction was conducted for 48 h at this temperature under continuous stirring (32 rpm). The reaction content was cooled to the room temperature and polymer precipitated was filtered and successively washed with tetrahydrofuran (20 mL), acetone (20 mL), and methanol (20 mL). The product was dried at 45°C under vacuum for overnight. The yield was 3 g (30%).

The residual double bonds on the surface of nearly monodisperse (~2.5 μm) (see Fig. 1b), PDVB microspheres were activated to primary bromine [66, 67] and then converted into azide functions by condensation with NaN_3. Finally, fluorescence labeled PDVB microspheres were obtained by the click reaction [68] with propargyl pyrene [69] through azide functions (Scheme 1).

Film Preparation

Composites were prepared by mixing of PMMA latex and pyrene labeled crosslinked PDVB microsphere. For this purpose, PMMA and PDVB particles were dispersed separately in heptane solutions. The dispersion of PDVB in heptane was mixed with the appropriate solutions of PMMA to yield eventually composites with 0, 1, 3, 5, 10, 20, 40, and 60 wt% PDVB content. Each mixture was stirred for 30min followed by sonication for 15 min at room temperature. The mixed dispersion was then coated on a glass plates with similar surface areas (0.8×2.5 cm^2) and allowed to dry under the ambient conditions of the laboratory. After drying, samples were separately annealed above T_g of PMMA for 10 min at temperatures ranging from 100 to 270°C. The temperature was maintained within ±2°C during annealing. After each annealing step, films were removed from the oven and cooled down to room temperature.

Measurements

After annealing, each sample was placed in the solid surface accessory of a Perkin-Elmer Model LS-50 fluorescence spectrometer. Pyrene (P) was excited at 345 nm and monomer and excimer fluorescence emission spectra were detected between 350 and 600 nm. All measurements were carried out in the front-face position at room temperature. Slit widths were kept at 8 nm during all SSF measurements. The sample position, incident light, I_0, I_P, and I_E emission intensities are shown in Fig. 2a.

Photon transmission experiments were carried out using Variant Carry-100 UV-Visible (UVV) spectrometer. The transmittances of the films were detected at 500 nm. A glass plate was used as a standard for all UVV experiments and measurements were carried out at room temperature after each annealing process. The sample position and the transmitted light intensity, I_{tr} are presented in Fig. 2b.

Scanning electron microscope (SEM) images were taken by using LEO Supra VP35 FESEM.

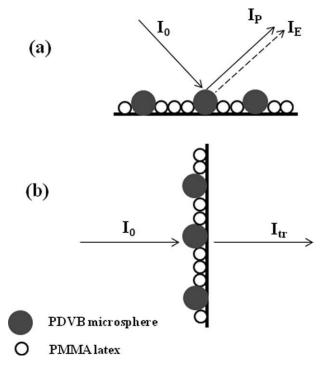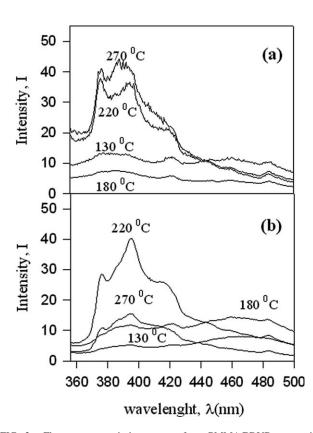FIG. 2. Schematic illustration of sample position and (a) incident light (I_0), monomer (I_P) and excimer (I_E) emission intensities, (b) transmitted light intensity (I_{tr}).
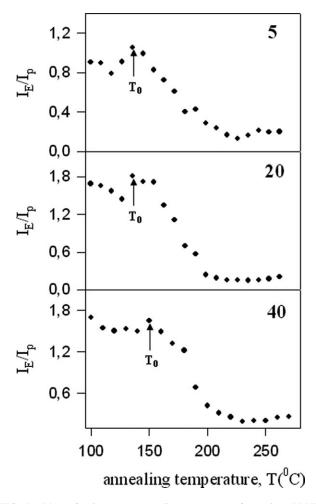

FIG. 3. Fluorescence emission spectra from PMMA/PDVB composite films for (a) 5 and (b) 40 wt%PDVB content after being annealed at various temperatures for 10 min. Numbers on each curve represent annealing temperatures.

RESULTS AND DISCUSSIONS

Preformed Excimers in Composite Film

Monomer and excimer emission spectra of 5 and 40 wt% PDVB content films annealed at elevated temperatures for 10 min are shown in Fig. 3a and b, respectively. At the beginning of annealing, monomer and excimer emission exist and their intensities are low for both film samples. However, at higher annealing temperatures, only the monomer emission appears and excimer emission is disappeared. In order to see the behavior of excimer (I_E) and monomer emission, I_E/I_P ratios versus annealing temperature, T were plotted for various PDVB content shown in Fig. 4. Here, it is seen that I_E/I_P ratio remains roughly unchanged below a certain temperature called minimum film formation temperature, T_o from which I_E/I_P ratio dramatically decreases by further annealing. The plot of I_E/I_P ratio against PDVB content is presented in Fig. 5. As can be seen that excimer formation is very low for the composites with low PDVB content and then increases for 20, 40, and 60 wt% PDVB content samples at annealing tem-

FIG. 4. Plots of I_E/I_P versus annealing temperature for various PDVB content blend films. Numbers on each curve represent PDVB content in the film. Here, T_0 is the minimum film formation temperature.
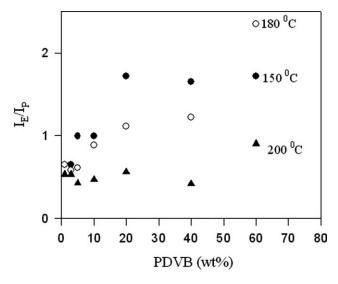
FIG. 5. Plots of I_E/I_P versus PDVB content for various annealing temperatures.

peratures below T_0. Above T_0 excimer formation starts to decrease and completely disappears above 200°C indicating completion of PMMA latex film formation process. In other words, above T_0 preformed intra and inter particle excimer of microspheres disappears due to interception of
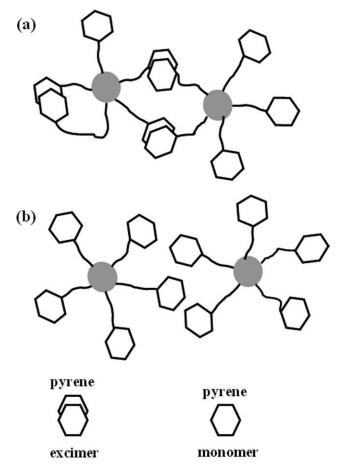

FIG. 6. Pictorial representation of intra and inter particle excimer formation in PMMA/PDVB film (a) below 200°C, (b) above 200°C.

PMMA chains in the interstitial domains between pyrenes. Schematic presentation of such particle excimers of PVDB microspheres below and above T_0 is given in Fig. 6.

Here, the simple Arrhenius treatment (see Fig. 7) may provide us with the energy need for the destruction of the preformed intra and inter particle excimer

$$I_E/I_P = \operatorname{Re} xp(-\Delta E/k_B T) \qquad (1)$$

where ΔE is the destruction energy for the excimer, which is related to both the polymer excimer interaction and the binding energy for the pyrenes involved in excimer unit. The produced ΔE values are given in Table 1. Expectedly, the destruction energy does not alter much by changing the PDVB content in the composite since ΔE is independent of the film composition.

Latex Film Formation

The change in transmittance of the composite films at 500 nm upon annealing are shown in Fig. 8 for 5, 20, and
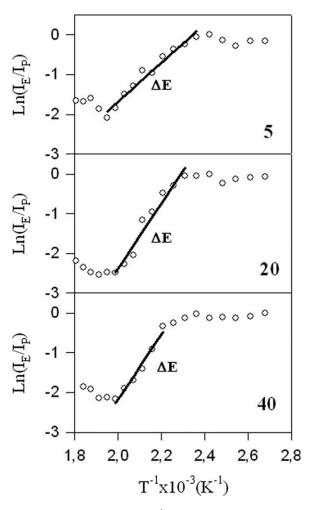

FIG. 7. Plots of Ln I_E/I_P versus T^{-1} curves and their fits to Arhenious equation. The slopes of straight lines produced excimer destruction (ΔE) energies. Numbers on each curve represents PDVB content in the film.

TABLE 1. Void closure (ΔH_{tr}), excimer destruction(ΔE) and interdiffusion (ΔE_{tr}) energies.

PDVB (wt%)	ΔE (kcal/mol)	ΔH_{tr} (kcal/mol)	ΔE_{tr} (kcal/mol)
0	–	1.58	11.04
1	14.02	8.34	10.57
3	7.68	9.33	11.78
5	9.66	2.66	8.30
10	11.12	4.4	7.21
20	16.29	2.89	6.06
40	16.27	4.22	7.48
60	8.69	1.04	17.55
Average	11.96	4.31	10.00

Standard deviations on; ΔE range from ± 0.61 to ± 1.33; ΔH_{tr} range from ± 0.16 to ± 0.35; ΔE_{tr} range from ± 0.56 to ± 2.2.

40 wt% PDVB content. All the curves in Fig. 8 have the same characteristic behavior. Upon annealing, the transmitted light intensity I_{tr} increases above the minimum film formation temperature, T_0 and then reaches a maximum. If the refractive indices of the two polymers are close, little scattering is expected. In general, light scattering is a function not only of the refractive index difference of the components but also of the size and shape of the dispersed-phase domains. Therefore, optical transmission measurements are a measure of the number and size of air voids in a polymer film [70]. Regardless of the void fraction, transmission decreases with increasing void radius. On the basis of the change of transmittance of the films, the structure evolution of the film could be described as follow: at low annealing temperatures, despite the refractive indices of two polymers are somewhat different [71], the transparency of the film is related to the size of the particles and voids inside the film which leads to light scattering. As the annealing temperature is increased, PMMA particles deform and flow into the voids resulting in disappearance of interparticle voids and flattening of the film. Therefore, transmittance of the film increases upon annealing due to homogenization during film formation [59–62]. Flow can also change the morphology of the polymer composite, causing separation of PDVB micro particles. It is shown that annealing the film at temperature over T_0 leads to deformation and coalescence of adjacent PMMA particles forming a continuous matrix. Moreover, it was found that annealing seemed to prevent coalescence at all of the crosslinked PDVB particles. After void closure is completed, further annealing at higher temperatures causes healing and interdiffusion processes between PMMA particles. In this case, PMMA particles undergo coalescence and take part in film forming process, and clearly acted as the continuous phase. On the other hand, no coalescence of the PDVB particles is expected as they are highly crosslinked. Apparently, they do not contribute to latex film formation but disperse in the PMMA continuous phase.

It has to be noted that I_{tr} decreases dramatically with increasing PDVB contents in the film. The low PDVB content blend films are optically more transparent than those with high PDVB content at all annealing temperatures. The transparency of the latex film is mainly determined by the scattering of the light that is dependent on the size of different polymer phases and the voids in the film [70]. When the size of polymer phases and the voids are bigger than the wavelength of irradiation light, the light scatters, and as a result, the transparency decreases. After the void closure process completed, scattering takes place predominantly from the submicron crosslinked PDVB particles in PMMA matrix. The plots of the maximum values of I_{tr}, $(I_{tr})_m$ versus PDVB content in Fig. 9 also confirms this hypothesis. As the PDVB content increased, $(I_{tr})_m$ decreased, indicating that low transparency occurs at higher PDVB content. Since the size of PDVB particles is large with respect to the wavelength of the visible light, the light is scattered resulting in low transparency in the film [72]. It should also be pointed out that the curve in Fig. 9 is just the reverse mode of the curve in Fig. 5.

The increase in I_{tr} may be interpreted by the mechanisms of void closure, healing and interdiffusion processes [73–75].
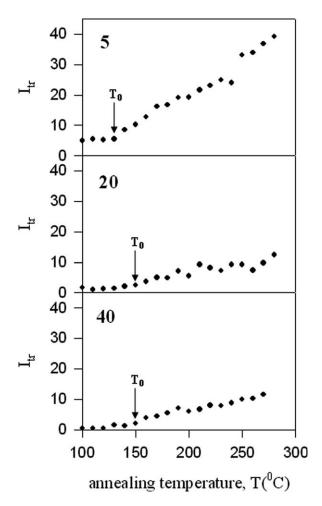

FIG. 8. Plots of transmitted photon intensities, I_{tr} vs. annealing temperatures, T, for the composite films contain 5, 20, and 40 wt%PDVB.
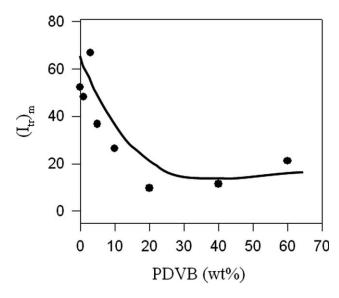
FIG. 9. Plot of the maxima of transmitted light intensities, $(I_{tr})_m$ versus PDVB latex content.

In order to gain more insight into these phenomena, the following mechanism and their formulations were proposed.

Particle Deformation and Voids Closure

To facilitate quantification of the behavior of I_{tr}, phenomenological void closure model can be introduced. Latex deformation and void closure between particles can be induced by shearing stress generated by surface tension of polymer, i.e., polymer-air interfacial tension. The void closure kinetics can determine the time for optical transparency and latex film formation [76]. In order to relate the shrinkage of spherical void of radius, r to the viscosity of surrounding medium, η an expression was derived and given by the following relation [76].

$$\frac{dr}{dt} = -\frac{\gamma}{2\eta}\left(\frac{1}{\rho(r)}\right) \qquad (2)$$

where γ is surface energy, t is time, and $\rho(r)$ is the relative density. It has to be noted that here surface energy causes a decrease in void size and the term $\rho(r)$ varies with the microstructural characteristics of the material, such as the number of voids, the initial particle size, and packing. If the viscosity is constant in time, integration of *Eq. 2* gives the relation as

$$t = -\frac{2\eta}{\gamma}\int_{r_o}^{r} \rho(r)dr \qquad (3)$$

where r_0 is the initial void radius at time $t = 0$.

The dependence of the viscosity of polymer melt on temperature is affected by the overcoming of the forces of macromolecular interaction which enables the segments of polymer chain to jump over from one equilibration position to another. This process happens at temperatures at which free volume becomes large enough and is con-

nected with the overcoming of the potential barrier. Frenkel-Eyring theory produces the following relation for the temperature dependence of viscosity [77, 78]

$$\eta = A \exp(\Delta H/kT) \qquad (4)$$

where ΔH is the activation energy of viscous flow, i.e., the amount of heat which must be given to one mole of material for creating the act of a jump during viscous flow. Here, A represents a constant for the related parameters which do not depend on temperature. Combining *Eqs. 3* and *4*, and assuming that the interparticle voids are in equal size and number of voids stay constant during film formation (i.e., $\rho(r) \propto r^{-3}$), then integration gives the following relation

$$t = \frac{2AC}{\gamma}\exp\left(\frac{\Delta H}{kT}\right)\left(\frac{1}{r^2} - \frac{1}{r_o^2}\right) \qquad (5)$$

Where, C is a constant related to relative density $\rho(r)$. As stated previously, decrease in void size (r) causes an increase both in I_{tr} ratios. Since the scattering intensity, I_s varies with volume squared ($I_s \propto v^2$) of the scattering object [79], it can be assumed that I_{tr} is inversely proportional to the sixth power of void radius, r. Thus, *Eq. 5* can be written as [73, 80]

$$I_{tr}(T) = S(t)\exp\left(-\frac{3\Delta H}{k_B T}\right) \qquad (6)$$

where $S(t) = (\gamma t/2AC)^3$. Here, r_0^{-2} is omitted since it is quite small compare to r^{-2} values after void closure process is started.

$$\mathrm{Ln}I_{tr}(T) = \mathrm{Ln}S(t) - \frac{3\Delta H}{k_B T} \qquad (7)$$

LnI_{tr} vs. T^{-1} plots of the data in Fig. 8 are presented in Fig. 10. All the plots in Fig. 10 present two linear regions, corresponding to void closure and interdiffusion processes, respectively. Intersections between the broken lines indicate the healing points (T_h). Data in Stage 1 in Fig. 10 are fitted to *Eq. 7*, and ΔH_{tr} values are obtained from the slopes. The resultant ΔH_{tr} values are listed in Table 1 for all the films with different PDVB content. The averaged ΔH_{tr} value was found to be 4.31 kcal/mol. It is seen that activation energies do not change much by increasing PDVB content. This means that the amount of heat which was required by one mole of polymeric material to accomplish a jump during viscous flow do not change by varying the film composition. It is, therefore, concluded that energy need for viscous flow of PMMA is not affected by PDVB microspheres.

Healing and Interdiffusion

The further increase in I_{tr} (Stage 2 in Fig. 10) can be explained by the increase in transparency of latex film
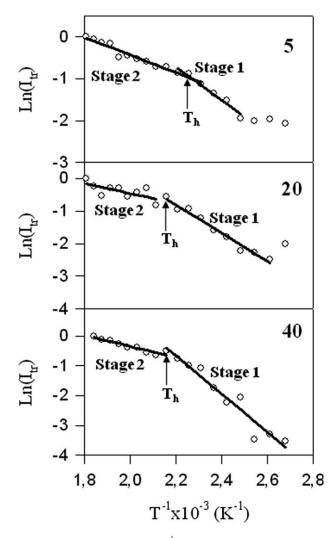
FIG. 10. Plots of Ln I_{tr} versus T^{-1} curves and their fits to *Eqs. 7* and *11*. The slopes of straight lines produced void closure (ΔH_{tr}) and inter-diffusion (ΔE_{tr}) energies. Stages 1 and 2 present the void closure and interdiffusion processes. Numbers on each curve represents PDVB content in the film.

from chains which have relaxed at least once. In terms of reduced time $\tau = 2vt/N^2$, the total crossing density can be given as [81, 82]

$$\sigma(\tau)/\sigma(\infty) = 2\pi^{-1/2}\tau^{1/2} \tag{8}$$

Here, N is the number of freely jointed segments and v is the linear diffusion coefficient given by the following relation

$$v = v_o \exp(-\Delta E/kT) \tag{9}$$

where ΔE is defined as the activation energy for backbone motion depending on the temperature interval. Combining *Eq. 8* and *Eq. 9* a useful relation is obtained as

$$\sigma(\tau)/\sigma(\infty) = R_o \exp(-\Delta E/2kT) \tag{10}$$

where $R_o = (8v_ot/\pi N^2)^{1/2}$ is a temperature independent coefficient. The increase in I_{tr} at Stage 2 in Fig. 8 is already related to the disappearance of particle–particle interface, i.e., as annealing temperature increased, more chains relaxed across the junction surface and as a result the crossing density increases. To explain the behavior of I_{tr} above T_h, it can be assumed that I_{tr} is directly proportional to the crossing density $\sigma(T)$. Then, *Eq. 10* can be solved for I_{tr} to interpret the results in Fig. 8 as follows:

$$I_{tr}(T)/I_{tr}(\infty) = \text{Re} \, xp(-\Delta E_{tr}/2kT) \tag{11}$$

The activation energy of backbone motion, ΔE_{tr} is produced by least squares fitting the data in Fig. 10 (Stage 2) to *Eq. 11*. ΔE_{tr} values are listed in Table 1. The average ΔE_{tr} value is found to be as 10.0 kcal/mol for transmission which are much larger than the void closure activation energies. This result is understandable because a single chain needs more energy to execute diffusion across the polymer–polymer interface than to be accomplished by the viscous flow process. The calculated activation energies were found roughly independent of PDVB content in the film.

Morphological Studies

To support these findings, SEM was used to examine the morphologies of PMMA/PDVB composite films. Figures 11–13 present SEM photographs of the films which have 0, 5, and 20 wt% PDVB content annealed at 100, 180, and 270°C, respectively. The SEM images of the films annealed at 100°C (Figs. 11a, 12a, and 13a) show that the surface of the composite films is very rough. These results reveal that 100°C, close to the T_g of PMMA, is too low to make the particles deform and retain their spherical shapes. Most of the light scatters due to the rough surface of the films which results low transmitted light intensity. Here, the small particles are PMMA latexes, while the large ones are crosslinked PDVB microspheres.

due to the disappearance of particle–particle boundaries known as interdiffusion. As the annealing temperature is increased above T_h, some part of the polymer chains may cross the junction surface and particle boundaries disappear, consequently, the transmitted photon intensity I_{tr} increases, whereas I_E decreases due to the disappearing of pyrene excimer. In order to quantify these results, the Prager-Tirrell (PT) model [81, 82] for the chain crossing density can be employed. These authors used de Gennes's "reptation" model to explain configurational relaxation at the polymer–polymer junction where each polymer chain is considered to be confined to a tube in which executes a random back and forth motion [82]. The total "crossing density" $\sigma(t)$ (chains per unit area) at junction surface was calculated by PT by taking into account of the contributions $\sigma 1(t)$ since chains still retain some portion of their initial tubes, and also a reminder the $\sigma 2(t)$ which comes
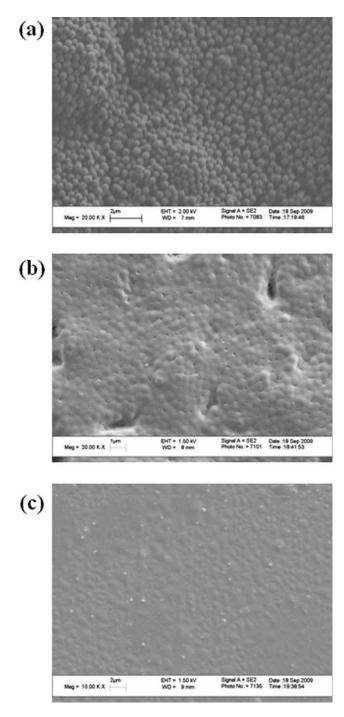
FIG. 11. Scanning electron micrographs (SEM) of pure PMMA films annealed at (a) 100°C, (b) 180°C, (c) 270°C for 10 min.

When the annealing temperature is 180°C which is much higher than the T_g of PMMA (see Figs. 11b, 12b, and 13b), the migration of PMMA latexes is accelerated. Hence, PMMA latex particles come into contact and spontaneously deform, which fill the interstitial space completely. Accordingly, the films become more flat and the voids between the particles are disappeared. However, at this temperature of annealing the PDVB particles seem to remain intact. The images in Fig. 11b show that film prepared from pure PMMA latex is flat and continuous,

whereas many cracks were observed in the films containing PDVB (Figs. 12b and 13b). This result reveals that the crosslinked PDVB latex is much harder than the PMMA latex and thus, cannot form film.

Annealing the films at 270°C (Figs. 11c, 12c, and 13c), the PMMA polymer chains in the particles start to flow and diffuse across the particle–particle interfaces, and the boundaries of PMMA particles are disappeared resulting in strengthening of the film. Despite the presence of some air bubbles pure PMMA film shows a regular and continuous surface structure. Interestingly, in films
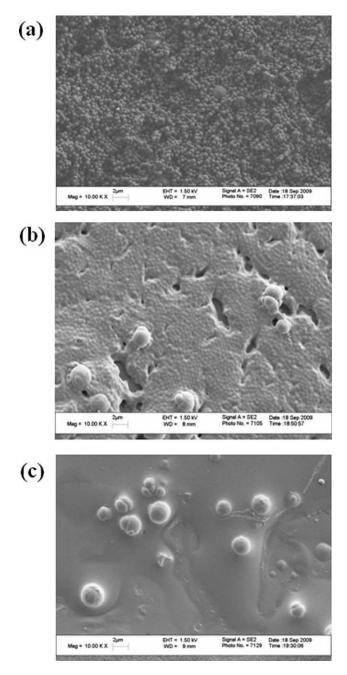

FIG. 12. Scanning electron micrographs (SEM) of composite films with 5 wt% PDVB annealed at (a) 100°C, (b) 180°C, (c) 270°C for 10 min.

FIG. 13. Scanning electron micrographs (SEM) of composite films with 20 wt% PDVB annealed at (a) 100°C, (b) 180°C, (c) 270°C for 10 min.

containing PDVB, cracks on the surface (Figs. 12c and 13c) disappear. Here again, the surface of the composite films having micrometer-sized PDVB particles seemed smooth and homogeneous (Figs. 12c and 13c). These images also indicate that no deformation occurs in PDVB particles, even at the highest annealing temperature. It is believed that, because of further annealing, small PMMA particles coalesce and coat the larger PDVB micropar-
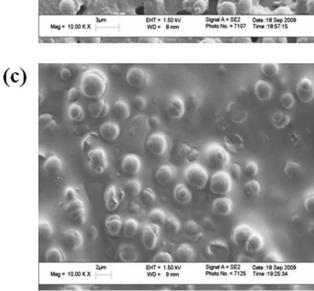
ticles forming a layer around them. In this way, PDVB microparticles are separated by the PMMA matrix. Similarly, most of the pyrenes pairs emitting solely excimer fluorescence (see Fig. 6) are also separated and pyrene units start to emit mostly excited state fluorescence (I_P) as reflected by the decrease in I_E/I_P ratio. These results clearly demonstrate that the morphological studies conducted by SEM analysis are in complete agreement with the interpretation of the I_{tr} and I_E/I_P behaviors of the samples presented in Fig. 6.
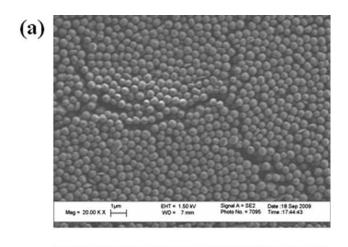
CONCLUSION

In conclusion, film formation process of PMMA/PDVB composites were investigated using excimer and monomer fluorescence from the pyrene labeled to PDVB microspheres, in conjugation with the morphological evolution of the films at elevated temperatures. It was found that annealing of these films led to coalescence of the PMMA particles resulting in a continuous PMMA matrix consist of microsized PDVB particles. SEM images of blend films confirmed that the PDVB particles which retain their identity were distributed within the PMMA matrix without aggregation. Upon annealing two different film formation stages, i.e. void closure and interdiffusion, were observed from I_{tr} data. It has been also shown that simple kinetic models for void closure and interdiffusion mechanisms are fitted quite well to the data. The related ΔH and ΔE activation energy values were not strongly affected by the PDVB content. Consequently, energy values appear to be relatively insensitive to film composition.

REFERENCES

1. H.D.H. Stöver and K. Li, In *Polymeric Materials Encyclopedia*, Salamone,J.C., Ed.; CRC Press: New York, 4519 (1996).

2. D. Horak, *Acta Polym.*, **47**, 20 (1996).

3. J. Ugelstad, H.R. Mfutakamba, P.C. Mørk, T. Ellingsen, A. Berge, R. Schmid, L. Holm, A. Jørgedal, F.K. Hansen, and K. Nustad, *J. Polym. Sci., Polym. Symp.*, **72**, 225 (1985).

4. R. Arshady, *Colloid Polym. Sci.*, **270**, 717 (1992).

5. K. Li and H.D.H. Stöver, *J. Polym. Sci., Part A: Polym. Chem.*, **31**, 3257 (1993).

6. C.H. Bamford, A. Ledwith, and P.K. Sen Gupta, *J. Appl. Polym. Sci.*, **25**, 2559 (1980).

7. W.H. Li and H.D.H. Stöver, *J. Polym. Sci., Part A: Polym. Chem.*, **36**, 1543 (1998).

8. Y. Naka, Kaetsu I., Y. Yamamoto, and K. Hayashi, *J. Polym. Sci., Part A: Polym. Chem.*, **29**, 1197 (1991).

9. M. Yoshida, M. Asano, I. Kaetsu, and Y. Morita, *Radiat. Phys. Chem.*, **30**, 39 (1987).

10. T.J. Romack, E.E. Maury, and J.M. DeSimone, *Macromolecules*, **28**, 912 (1995).

11. S. Sosnowski, M. Gadzinowski, and S. Slomkowski, *Macromolecules*, **29**, 4556 (1996).

12. H.D.H. Stöver and K. Li, In *Polymeric Materials Encyclopedia*, J.C. Salamone, Ed.; CRC Press: New York, 7237 (1996).

13. J.S. Downey, R.S. Frank, W.-H. Li, and H.D.H. Stöver, *Macromolecules*, **32**, 2838 (1999).

14. H.C. Kolb, M.G. Finn, and K.B. Sharpless, *Angew. Chem., Int. Ed.*, **40**, 2004 (2001).

15. C.W. Tornoe, C. Christensen, and M. Meldal, *J. Org. Chem.*, **67**, 3057 (2002).

16. A.S. Goldman, A. Walther, L. Nebhani, R. Joso, D. Ernst, K. Loos, C. Barner-Kowollik, L. Barner, and A.H.E. Muller, *Macromolecules*, **42**, 3707 (2009).

17. B. Karagoz, Y.Y. Durmaz, B.N. Gacal, N. Bicak, and Y. Yagci, *Des. Mon& Polym.*, **12**, 511 (2009).

18. T.-W. Chou, "Structure and Properties of Composites," in *Materials Science and Technology*, R.W. Cahn, P. Haasen, and E.J. Kramer, Eds., VCH Weinheim, Vol 13 (1993).

19. M.A. Winnik, *Curr. Opin. Colloid Interface Sci.*, **2**, 192 (1997).

20. A. Toussaint and M.D. Wilde, *Prog. Org. Coat.*, **30**, 113 (1997).

21. S.G. Croll, *J. Coat. Technol.*, **58**, 41 (1986).

22. J.L. Keddie, *Mater. Sci. Eng.*, **R21**, 101 (1997).

23. T. Provder, M.A. Winnik, and M.W. Urban, Film Formation in Waterborne Coatings, ACS Symp., Amer. Chem. Soc. Ser. 648, Washington D.C. (1996).

24. P.R. Sperry, B.S. Snyder, M.L. O'Dowd, and P.M. Lesko, *Langmuir*, **10**, 2619 (1994).

25. J.K. Mackenzie and R. Shuttleworth, *Proc. Phys. Soc.*, **62**, 838 (1949).

26. J.N. Yoo, L.H. Sperling, C.J. Glinka, and A. Klein, *Macromolecules*, **24**, 2868 (1991).

27. Ö. Pekcan, *Trends Polym. Sci.*, **2**, 236 (1994).

28. S. Ugur and O. Pekcan, *Colloid Polym. Sci.*, **284**, 309 (2005).

29. D.B. Otts, S. Dutta, P. Zhang, O.W. Smith, S.F. Thames, and M.W. Urban, *Polymer*, **45**, 6235 (2004).

30. Y.J. Park, M.C. Khew, C.C. Ho, and J.H. Kim, *Colloid Polym. Sci.*, **276**, 709 (1998).

31. F. Huijs and J. Lang, *Colloid Polym. Sci.*, **278**, 746 (2000).

32. D. Colombini, N. Ljungberg, H. Hassander, and O.J. Karlsson, *Polymer*, **46**, 1295 (2005).

33. J.T. Byers and MP Wayner. In *Rubber Technology*, 3rd ed., MortonM, Ed., Van Nostrand Reinhold, New York, [chapter 3] (1987).

34. S. Wolff and M.-J. Wang, *Rubber Chem. Technol.*, **65**, 329 (1992).

35. S. Agarwal and R. Salovey, *Polym Eng. Sci.*, **35**, 1241 (1995).

36. J. Zhu, Y.-C. Ou, and Y.-P. Feng, *Polym. Int.*, **37**, 105 (1995).

37. A.B. Metzner, *J. Rheol.*, **29**, 739 (1985).

38. M.R. Kamal and A. Mutel, *J. Polym. Eng.*, **5**, 293 (1985).

39. U. Yilmazer and R.J. Farris, *J. Appl. Polym. Sci.*, **28**, 3369 (1983).

40. M. Park, K. Gandhi, L. Sun, R. Salovey, and J.J. Aklonis, *Polym. Eng. Sci.*, **30**, 1158 (1990).

41. L. Sun, M. Park, J.J. Aklonis, and R. Salovey, *Polym. Eng. Sci.*, **32**, 1418 (1992).

42. L. Sun, J.J. Aklonis, and R. Salovey, *Polym. Eng. Sci.*, **33**, 1308 (1993).

43. J.J. Cai and R. Salovey, *J. Polym. Sci. Part B Polym. Phys.*, **37**, 815 (1999).

44. O. Nuyken and R. Bayer, *Kautsch Gummi Kunstst*, **48**, 704 (1995).

45. Z. Yang, A. Merrington, and D.J. Meier, *Polym. Mater. Sci. Eng.*, **73**, 438 (1995).

46. G. Lindenblatt, W. Schärtl, T. Pakula, and M. Schmidt, *Macromolecules*, **34**, 1730 (2001).

47. X. Wang, J.E. Hall, S. Warren, J. Krom, J.M. Magistrelli, M. Rackaitis, et al. *Macromolecules*, **40**, 499 (2007).

48. X. Wang, V.J. Foltz, M. Rackaitis, and G.G.A. Böhm, *Polymer*, **49**, 5683 (2008).

49. O.W. Burke, *Br. Pat.*, **043**, 799 (1958).

50. S. Mani, M.F. Malone, H.H. Winter, J.L. Halary, and L. Monnerie, *Macromolecules*, **24**, 5451 (1991).

51. F.B. Cheikh Larbi, M.F. Malone, H.H. Winter, J.L. Halary, M.H. Leviet, and L. Monnerie, *Macromolecules*, **23**, 3534 (1988).

52. F. Amrani, J.M. Hung, and H. Morawetz, *Macromolecules*, **13**, 649 (1980).

53. H. Morawetz, *Polym. Eng. Sci.*, **23**, 689 (1983).

54. J.B. Birks, *Photophysics of Aromatic Molecules*, Wiley, New York, Chapter 7(1970).

55. J.B. Birks and L.G. Christophoron, *Proc. Roy. Soc.*, **A274**, 552 (1963).

56. C. Cuniberti and A. Perico, *Eur. Polym. J.*, **13**, 369 (1977).

57. M.A. Winnik and T. Redpath, *Macromolecules*, **13**, 328 (1980).

58. L.S. Egan, M.A. Winnik, and M.D. Crouche, *Polym. Eng. Sci.* **26**, 15 (1986).

59. Ş. Uğur, A. Elaissari, and Y. Holl, *Polymer Composites*, **27**, 431 (2006).

60. Ş. Uğur and Y. Holl, *e-Polymers*, **037**, 1 (2006).

61. Ş. Uğur, M.S. Sunay, A. Elaissari, and O. Pekcan, *Polym Compos*, **31**, 1637 (2010).

62. Ş. Uğur, M.S. Sunay, and O. Pekcan, *Polym. Compos* **31**, 1611 (2010).

63. O. Pekcan, M. A. Winnik, and L. Egan, *Macromolecules*, **16**, 702 (1983).

64. M.A. Winnik, Ö. Pekcan, and L. Egan, *Polymer* **25**, 1767 (1984).

65. M.A. Winnik, Ö. Pekcan, and L. Chen, *Macromolecules* **21**, 55 (1988).

66. F. Lime and K. Irgum, *J. Polym. Sci., Part A: Polym. Chem*, **47**, 1259 (2009).

67. A. Nyhus, S. Hagen, and A. Berge, *J. Polym. Sci., Part A: Polym. Chem.*, **38**, 1366 (2000).

68. B. Karagoz, Y.Y. Durmaz, N.B. Gacal, N. Bicak, and Y. Yagci, *Des. Mon& Polym.*, **12**, 511,(2009).

69. B.N. Gacal, B. Koz, B. Gacal, B. Kiskan, M. Erdogan, and Y. Yagci, *J. Polym. Sci., Part A: Polym. Chem*, **47**, 1317 (2009).

70. G.H. Meeten, *Optical Properties of Polymers*, Elsevier Applied Science Publishers, London, 29 (1986).

71. L. Bohn, in *Polymer Handbook*, 2nd ed., J. Brandup and E.H. Immergut, Eds., Wiley-Interscience, New York, 1975.

72. J.L. Keddie, P. Meredith, R.A.L. Jones, and A.M. Donald, *Langmuir*, **12**, 3793 (1996).

73. Ş. Uğur, A. Elaissari, and Ö. Pekcan, *J. Coll. Int. Sci.*, **263**, 674 (2003).

74. Ş. Uğur, A. Elaissari, and Ö. Pekcan, *J. Coat. Technol. Res.*, **1**(4), 305 (2004).

75. Ö. Pekcan and E. Arda, *Colloids Suf. A*, **153**, 537 (1999).

76. J.L. Keddie, P. Meredith, R.A.L Jones, and A.M. Donald, in *Film Formation in Waterborne Coatings*, T. Provder, M.A. Winnik and M.W. Urban (Eds.), ACS Symp. Ser. 648, American Chemical Society, 332 (1996).

77. G.S. Fulcher, *J. Am. Ceram. Soc.*, **8**, 339 (1925).

78. J. Frenkel, *J. Phys. USSR*, **9**, 385 (1945).

79. S.S. Voyutskii, *Collois Chemistry*, MR Publisher, Moscow(1978).

80. Ş. Uğur, A. Elaissari, and Ö. Pekcan, *Polym. Adv. Technol.*, **16**, 405 (2005).

81. S. Prager and M. Tirrell, *J. Chem. Phys.*, **75**, 5194 (1981).

82. R.P. Wool, B.L. Yuan, and O.J. McGarel, *J. Polym. Eng. Sci.*, **29**, 1340 (1989).